frontiers | Frontiers in Energy Research

ORIGINAL RESEARCH
published: 12 July 2022
doi: 10.3389/fenrg.2022.925430

Improved Lifetime of Na-Ion Batteries With a Water-Scavenging Electrolyte Additive

Lin Chen[1†], Brij Kishore[1†], Tengfei Song[1], Marc Walker[2], Claire Dancer[3] and Emma Kendrick[1*]*

[1]School of Metallurgy and Materials, University of Birmingham, Birmingham, United Kingdom, [2]Department of Physics, University of Warwick, Coventry, United Kingdom, [3]Warwick Manufacturing Group, University of Warwick, Coventry, United Kingdom

The lifetime of sodium-ion batteries is strongly affected by degradation species and contaminants such as H_2O and HF, which are produced during formation and cycling. In this work, the use of low levels of N, N-diethyltrimethylsilylamine (DETMSA), as an electrolyte additive, shows an improvement in the stability and cycle life of a hard carbon vs. layered oxide sodium-ion battery. Approximately 80% of the capacity is retained after 500 cycles, which is almost double the performance of the standard electrolyte. The additive works by reducing the surface ageing constituents, as observed through XPS of the surfaces and the change in resistance after cycling. DETMSA is slowly consumed over time; however, the extensive improvement in cycle life shows that low level of impurities and degradation species have a big impact upon cycle life.

Keywords: sodium-ion battery, electrolyte additives, Si–N bond, H_2O and HF, lifetime

OPEN ACCESS

Edited by:
Montserrat Galceran Mestres, CIC energigune, Spain

Reviewed by:
Xiaoen Wang, Deakin University, Australia
Xia Li, Concordia University, Canada

***Correspondence:**
Lin Chen
l.chen.5@bham.ac.uk
Emma Kendrick
e.kendrick@bham.ac.uk

[†]These authors have contributed equally to this work

Specialty section:
This article was submitted to Electrochemical Energy Conversion and Storage, a section of the journal Frontiers in Energy Research

Received: *21 April 2022*
Accepted: *31 May 2022*
Published: *12 July 2022*

Citation:
Chen L, Kishore B, Song T, Walker M, Dancer C and Kendrick E (2022) Improved Lifetime of Na-Ion Batteries With a Water-Scavenging Electrolyte Additive. Front. Energy Res. 10:925430. doi: 10.3389/fenrg.2022.925430

INTRODUCTION

A holistic approach to the sustainability of sodium-ion batteries (NIB) considers the material components, cost/energy for manufacturing, cell life-time, in-use conditions, and economic viability for material recovery at the end of life. In most cases, the lower cost of material components in NIB means that the 'sustainability' of the battery relies upon the cells being in use for a long time, as the value of the material components from recycling is very low, meaning recycling is economically unviable. Therefore, understanding and reducing the ageing mechanisms and degradation in NIB is paramount to producing long-lived cells.

Although NIB is a drop-in technology to lithium-ion batteries (LIB), there are notable differences around the stability of carbonate-based electrolytes in the cell and the associated solid electrolyte interface (SEI) (Single et al., 2016; Nayak et al., 2018; Xu et al., 2018; Fondard et al., 2020). As has been shown previously, in both cases, water is known to be detrimental to the performance and life-time of the cell, although possibly to a greater degree in NIB (Herriot; Yamane et al., 2001; Li et al., 2009; Wotango et al., 2017; Han et al., 2015; Chen et al., 2017). In the Li/$NaPF_6$ salt-based carbonate electrolytes and as a consequence of the H_2O in the battery, hydrofluoric acid (HF) is inevitably produced during cycling resulting in 1) the hydrolysis of the Li/$NaPF_6$ salt (**Eq. 1**) and 2) the decomposition of Li/$NaPF_6$ (**Eqs. 2**, **3**) (Herriot; Han et al., 2020; Zhang et al., 2022; Liao et al., 2021). The presence of HF, in particular, leads to a decrease in battery life, and this has been attributed to several mechanisms; transition metal (TM) loss from the cathode, current collector corrosion, and an increase in SEI on the anode.

$$\mathrm{Li/NaPF_6} + \mathrm{H_2O} \leftrightarrow \mathrm{Li/NaF} + 2\mathrm{HF} + \mathrm{POF_3}, \quad (1)$$

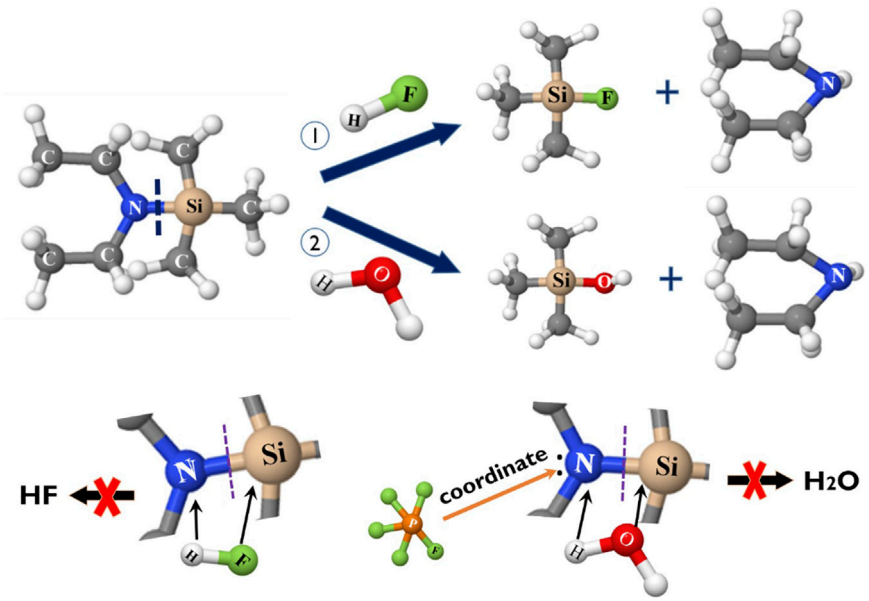

FIGURE 1 | The molecule structure of DETMSA and the reactions (1) with HF and (2) with H_2O by breaking the Si–N bond.

$$Li/NaPF_6 \leftrightarrow Li/NaF + PF_5, \quad (2)$$

$$H_2O + PF_5 \leftrightarrow 2HF + POF_3. \quad (3)$$

Both H_2O and HF have been identified as harmful species in batteries and their effects have been discussed extensively in the literature (Yamane et al., 2001; Li et al., 2009; Han et al., 2015; Single et al., 2016; Chen et al., 2017; Peebles et al., 2017; Wotango et al., 2017; Nayak et al., 2018; Han et al., 2019; Chen et al., 2020a; Fondard et al., 2020; Herriot, 2012; Han et al., 2020; Cheng et al., 2021; Haridas et al., 2021; Liao et al., 2021; Zhang et al., 2022).

Electrolyte filling in NIB cells is usually done in the glovebox (H_2O < 0.1 ppm) or dry room, which still contains low levels of water. H_2O can also be introduced *via* the low levels present in the electrolyte, from insufficiently dried components or from the electrolyte's decomposition. The moisture content in commercial electrolyte is typically controlled to less than 10 ppm, which means the main source of water in NIB cells is likely introduced during the manufacturing processes or generated in the battery itself, particularly during charging and especially during occasional overcharging (Zhang, 2006; Chang et al., 2020).

Previously, nanozeolite ZSM-5 was successfully introduced as an additive into the electrolyte to absorb small but harmful species like water, CO_2, and HF during cycling (Chen et al., 2020b). In this work, different from the physical absorption that nanozeolite can provide, a solution to extend the lifetime of NIBs by chemically scavenging the H_2O and subsequent HF is introduced, using a Lewis-base N, N-diethyltrimethylsilylamine (DETMSA) as an electrolyte additive. The Si–N bond contained within DETMSA is easily cleaved through reaction with Lewis acids such as HF or H_2O, as shown in **Figure 1** (Zhang, 2006; Han et al., 2020). Similar chemicals that contain Si–N bonds such as hexamethyldisilazane (HMDS) (Yamane et al., 2001), heptamethyldisila-zane (HTMDS) (Li et al., 2009), N, N-diethylamino trimethylsilane (DEATMS) (Chen et al., 2017; Zhou et al., 2018), (trimethylsilyl)isothiocyanate (TMSNCS) (Han et al., 2020), and 1-(trimethylsilyl)imidazole (1-TMSI) (Wotango et al., 2017) have been introduced into LIBs to enhance the cycling stability. DETMSA, the additive we selected in this work, is functionalized with a diethylaminol group, Si–N bond, and trimethlsilyl. The diethylamino group can increase the HOMO energy of the molecules and be preferentially oxidized, while the trimethylsilyl group does not have any negative effect (**Figure 1**) (Zhang, 2006; Zhou et al., 2018). Here, the cell cycling is improved when using DETMSA as an electrolyte additive. The changes in the interface layers on the hard carbon (HC) anode in an NIB full-cell configuration (transition metal oxide $NaMO_2$ as cathode) are investigated.

EXPERIMENT

Electrolyte Preparation

The standard electrolyte, 1 M $NaPF_6$ in EC: DEC (1/1, V/V) was purchased from Flurochem. To compare with the previous work (Chen et al., 2020b), we chose the same additive content. 1 wt% DETMSA additive (98%, Sigma-Aldrich) was directly added to the standard electrolyte by stirring manually. All the electrolyte preparation processes were completed in the glovebox (H_2O < 0.1 ppm, O_2 < 0.1 ppm).

Electrochemical Measurements of $NaMO_2$/HC Full Cells

Na_a $[Ni_wMn_xMg_yTi_z]O_2$ ($NaMO_2$), a mixed P2-O3 type oxide material (Bauer et al., 2018; Sayers et al., 2018), was made into an electrode with 92 wt% active material, 5 wt% conductive additive,

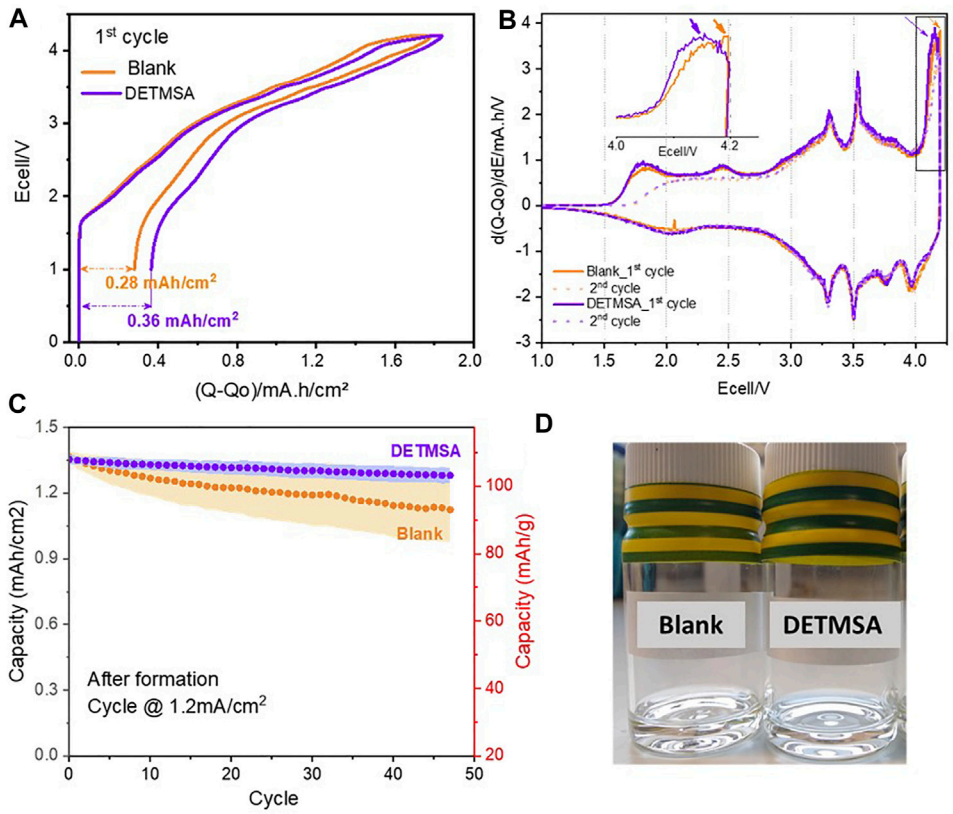

FIGURE 2 | (A).First charge/discharge profile. **(B)** Differential capacity (dQ/dV) plots and **(C)** cycling performances of the full cell with blank electrolyte and DETMSA electrolyte. **(D)** Images of freshly prepared electrolytes with and without DETMSA.

and 3 wt% PVDF binder using a slurry cast process. A hard carbon (Kuranode, Kurary) negative electrode was made (88 wt% active material: 9 wt% PVDF binder: 3 wt% carbon black). All the electrodes were dried in a vacuum oven at 120°C overnight prior to being transferred into a glovebox.

For the full cell assembly process, the mass balancing of positive and negative electrodes was calculated based on the $(N/P)_Q$ capacity ratio of 1.1:1. The electrochemical performance of the full cells was evaluated in a 2032-type coin cell, with $NaMO_2$ cathode (12 mg/cm^2), hard-carbon anode (5 mg/cm^2), separated by Celgard polymer 2325 containing enough electrolyte to wet the components (~75 µl or ~43.6 µl/cm^2). Each electrochemical test was performed using three independently produced cells to show standard deviations.

Surface Characterisation

After completion of cycling, the cell was disassembled in a glovebox under an argon atmosphere. Scanning electron microscopy with a field-emission SEM microscope (Sigma, Carl Zeiss, Germany) equipped with an energy-dispersive spectrometer (EDS) (Xmax 50, Oxford Instruments) was used to characterise the surface of the electrodes after cycling. SEM images were captured at 10 kV (1.6 nA) when a high-performance ion conversion and electron detector was used, or at 20 kV (8.0 nA) when a secondary electron detector was used.

X-ray photoelectron spectroscopy (XPS) measurements were carried out using a Kratos Axis Ultra DLD spectrometer (Kratos Analytical, Manchester, United Kingdom). Samples were prepared in an argon glovebox, mounted on a copper stub and transferred to the spectrometer using an inert transfer unit under an argon atmosphere with no exposure to air. Once an acceptable vacuum level had been reached, the samples were transferred to the main analysis chamber. The samples were illuminated by a monochromated Al Kα X-ray source (hν = 1486.7 eV) and flooded with low-energy electrons from a charge neutraliser to prevent the surface from becoming positively charged during the experiment. Data were collected in a hemispherical analyser using a pass energy of 160 eV for survey spectra and 20 eV for high-resolution core-level spectra (resolution approximately 0.4 eV). Data were analysed using the CasaXPS software package, using mixed Gaussian–Lorentzian (Voigt) lineshapes, asymmetry parameters where appropriate, and Shirley backgrounds. The spectrometer was calibrated using the Ag $3d_{5/2}$ peak and Fermi edge of clean polycrystalline Ag prior to the start of the experiment, with the transmission function determined using various clean metallic foils. The binding energies of the data were adjusted during the analysis, using the C-C/C-H component in the C 1*s* region at 285.0 eV as the reference point.

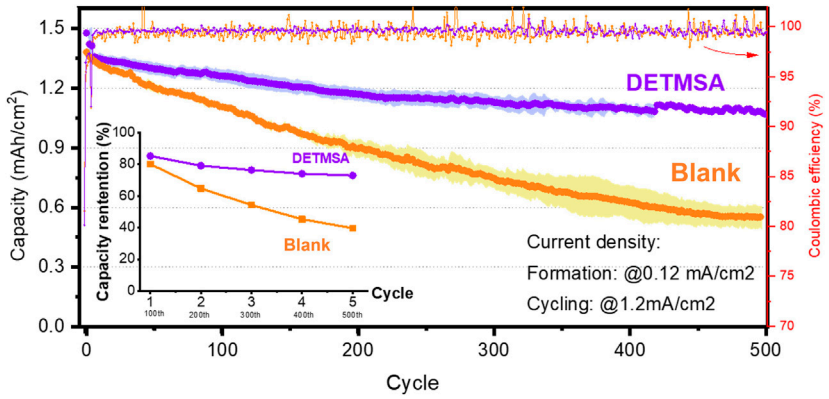

FIGURE 3 | The capacity performance of the full cell using different additives. Capacity retention after 100, 200, 300, 400, and 500 cycles at 1.2 mA/cm^2 after 5 cycles of formation process at 0.12 mA/cm^2.

RESULTS AND DISCUSSIONS

The effect of DETMSA additive on the cycling performance is shown in **Figure 2**. Following coin cell assembly, all cells were subjected to formation cycles where a small current of 0.12 mA/cm^2 (10 mA/g) was applied to generate an SEI layer between 1.0–4.2 V. The first charge–discharge curves are shown in **Figure 2A**, similar initial charge capacities 1.77 and 1.84 mA h/cm^2 (150 mA h/g), and first discharge capacities of ~1.49 mA h/cm^2 were observed for both cells, as expected for these cathode materials. The cell assembled with DETMSA electrolyte shows slightly more irreversible capacity. Differential capacity (dQ/dV) plots for the first and second cycle of the $NaMO_2$/HC cells were obtained to study electrolyte oxidation/reduction behaviour with the standard and DETMSA electrolytes as shown in **Figure 2B**. The plots were similar regardless of the presence of DETMSA, and no additional peaks were observed. The peak around 4.2 V shifted to a slightly lower potential in the cells assembled with DETMSA, as shown in **Figure 2B**. Considering the diethylamino group can increase the HOMO energy of the molecules and be preferentially oxidized, this shift may correspond to the decomposition of DETMSA (Chen et al., 2017). With increasing DETMSA concentrations, this shift increases, as shown, when comparing 0.5wt%, 1wt%, and 3wt% of DETMSA (**Supplementary Figure S0**). The electrochemical performances of $NaMO_2$/HC cells at higher rates (0.8 C) for ageing, after 5 cycles of formation processes, are displayed in **Figure 2C**. The cells start with similar initial areal capacities, being 1.36 and 1.35 mA h/cm^2, respectively, when they were cycled from 1.0 to 4.2 V at 0.8 C (1.2 mA/cm^2). The presence of DETMSA helped to reduce the capacity fading from 0.26% (for blank electrolyte) to 0.15% per cycle. In addition, the standard deviation of the results is significantly reduced with the DETMSA addition compared to the blank electrolyte, as shown in **Figure 2C**. As shown in **Supplementary Figure S0**, for increasing electrolyte additive concentrations, the first cycle loss increases as expected from the additive decomposition. In terms of cycling behaviour, 0.5wt% additive exhibits results very similar to the 1wt%, whereas the 3wt% fades faster. This indicates that small quantities of additive are beneficial, whereas larger levels are not. The images of the freshly prepared electrolyte with and without DETMSA are shown in **Figure 2D**. Both the electrolytes are very clear. Tests were performed on the electrolytes by heating them to 40°C and adding 4000 ppm of water. The electrolyte without DETMSA becomes hazier in both the experiments, as seen in **Supplementary Figure S1**, indicating an instability of the electrolyte which contains water. Previous work with lithium-ion electrolyte stability also shows etching of the glass vials over time, indicating HF presence (Gorman et al., 2019).

The long-term effect of DETMSA additive in the NIB full-cell system compared with a blank electrolyte are presented in **Figure 3**. After 5 cycles of standard formation process at 0.12 mA/cm^2 (0.08 C), the cells were cycled at 1.2 mA/cm^2 (0.8 C) for ~500 cycles between 1.0–4.2 V. As expected, a similar capacity fading phenomenon as presented in the 50-cycle data (in **Figure 2C**) is observed with all electrolytes. DETMSA aids cycle stability, and the capacity retention after 100, 200, 300, 400, and 500 cycles is compared and visually presented in **Figure 3**. The DETMSA additive yielded remarkably improved capacity retention of 73% compared to 39% in the blank electrolyte case.

The cells were de-crimped inside the glovebox after 500 cycles. The images of the hard-carbon negative electrodes are presented in **Supplementary Figure S2**. The shiny decomposition product on the anode edges is metallic sodium plating, which is much less visible with the presence of DETMSA, as presented in **Supplementary Figures S2a and S2d**. This demonstrates that the additive helps prevent Na plating.

Supplementary Figures S2b, c, e, and f show the morphologies of the non-plating and plating areas on the hard carbon after cycling 500 times at 1.2 mA/cm^2 charge/discharge rate. As a result of long-term cycling, the particles appeared to have more frayed edges with blank electrolyte (**Supplementary Figure S2b**) compared to the one with DETMSA (**Supplementary Figure S2e**). Surface cracking was even observed in the plating area in the sample without DETMSA, as shown in **Supplementary Figure S2c**. The microstructural

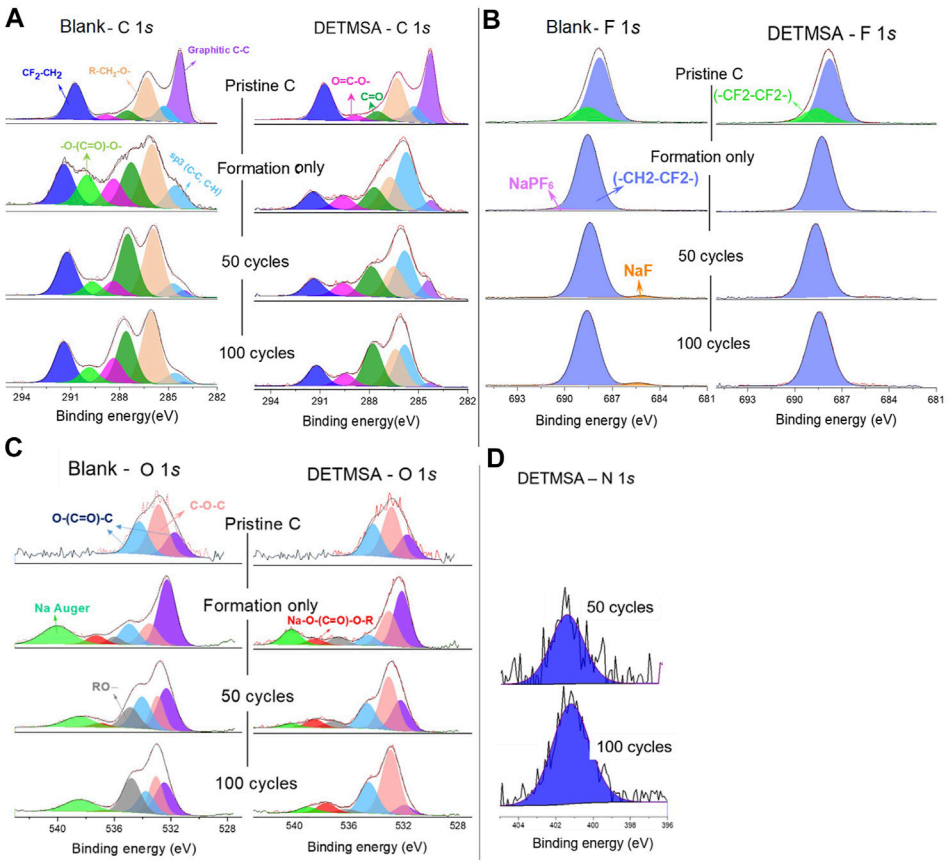

FIGURE 4 | The XPS spectra of pristine hard-carbon electrodes and those electrodes after formation, after 50 cycles, and after 100 cycles by using blank and DETMSA electrolytes. **(A)** the C 1s, **(B)** O 1s, **(C)** F 1s, and **(D)** N 1s spectra of the hard-carbon electrodes.

observations reveal that the electrolyte with additive DETMSA is more beneficial in forming a more stable surface on the anode compared to the blank electrolyte without additive.

XPS was performed to give greater insight into the combination of compounds which comprise the SEI layer formed on the anode after formation, 50 cycles, and 100 cycles. Results are presented in **Figures 4A–D**, and all peaks are normalised to a standard. As discussed in our previous article (Chen et al., 2020b), different bonding environments arising from the different electrolyte decomposition products were present in the cycled anodes. The C 1s spectra show the peaks corresponding to the sp^3 C–C bonds of hard carbon (285.0 eV), the C–O bond in sodium alkyl carbonate (Na-O-(C=O)-O-CH_2-R, 286.2 eV, pale orange peak), and the C atom in the carbonate coordination in sodium alkyl carbonate (Na-O-(C=O)-O-CH_2-R, 289.2 eV, magenta peak) in pristine hard-carbon electrodes (Jiang et al., 2018; Wotango et al., 2018; Eshetu et al., 2019; Kim et al., 2019; Yan et al., 2019). These findings are also reflected in the O 1s spectra in which the peaks observed at ~532 and ~534 eV are believed to correspond to O atoms in sodium alkyl carbonate 26. The C 1s core spectra reveal, upon cycling, the appearance of a new peak located at 290.4 eV (light green in **Figure 4A**), which is assigned to Na_2CO_3. This peak was not detected in the DETMSA-containing electrolyte, which indicates a lower degree of electrolyte decomposition had occurred with the addition of DETMSA. This is also confirmed from the lower density of the pale orange peak (Na-O-(C=O)-O-CH_2-R, 286.2 eV) in DETMSA-containing electrolyte, which corresponds to sodium alkyl carbonate. These indicate DETMSA aids in providing a thinner inorganic inner SEI layer on the hard-carbon surface than blank electrolyte. The same trend of the –O-(C=O)-O peak in blank and DETMSA electrodes in C 1s spectra (**Figure 4A**, light green) also applied to the Na Auger peak in O 1s spectra in **Figure 4C** (light green) since the Na Auger emission arising from both Na_2CO_3 and sodium alkyl carbonate. The peak observed at ~536 eV (grey peak) is believed to correspond to the O atoms in organic species arising from the decomposition of the electrolytes. The low intensities of the grey peak in DETMSA electrolyte indicate a lower concentration of organic species is present within the SEI.

The peaks at ~685 eV (orange peak) in F 1s spectra which appeared in the cycled electrodes with blank electrolyte are attributed to NaF, derived from $NaPF_6$ decomposition (Chen et al., 2020b; Gorman et al., 2019; Kim et al., 2019; Jiang et al., 2018). This decomposition is suppressed with the addition of an additive, as there are no NaF peaks detected in the DETMSA-

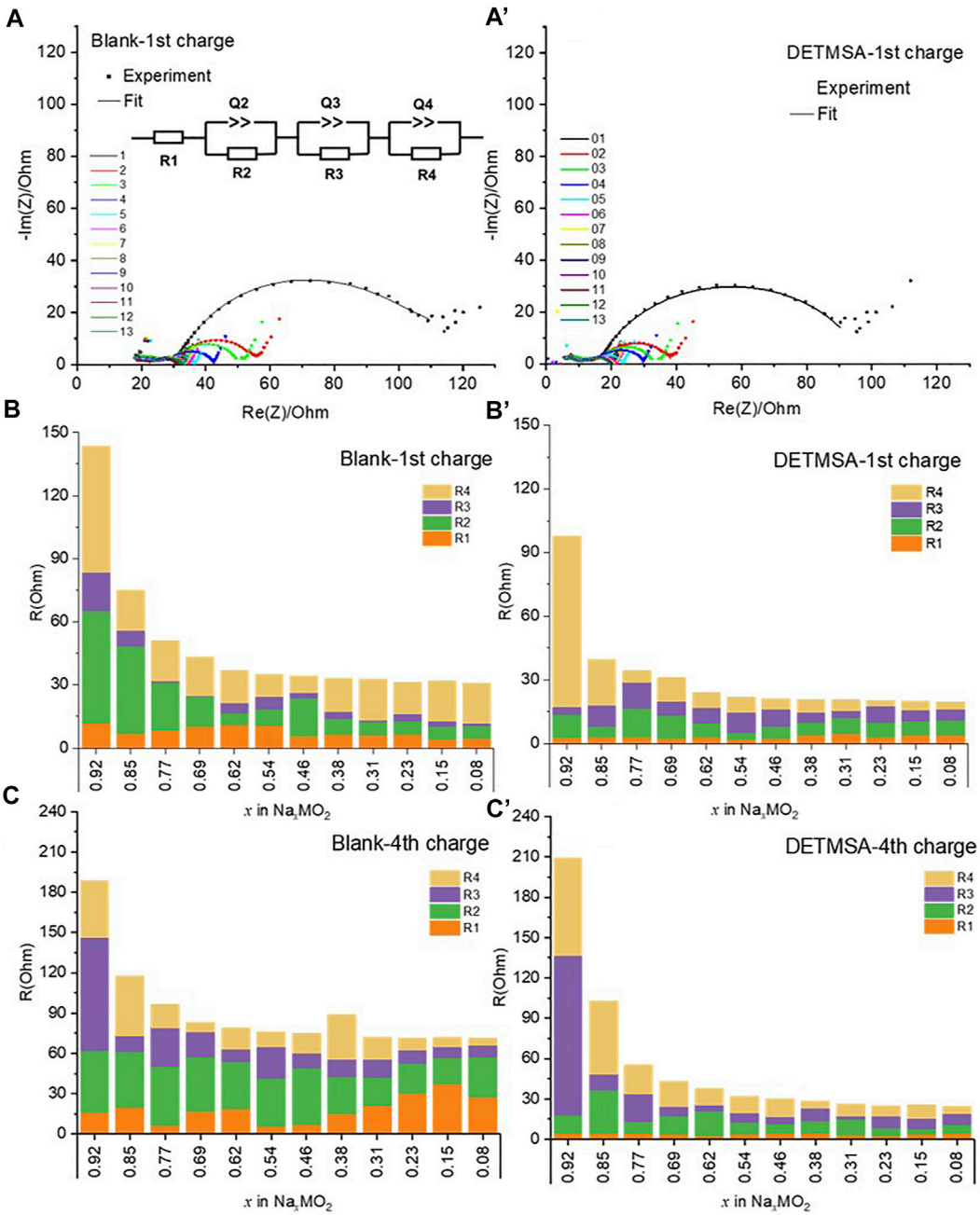

FIGURE 5 | Impedance spectra (1–10 mHz) of $NaMO_2$/HC at different states of charge (SOC = 100–0%) during the first and fourth charging processes and the resistance parameters at different x values in $NaxMO_2$ with different electrolytes: **(A)**, **(B)**, and **(C)** with blank electrolyte; **(A')**, **(B')**, and **(C')** with DETMSA electrolyte.

containing electrolyte, as shown in **Figure 4B**, which is consistent with the previous discussions.

The N 1s peak (**Figure 4D**) intensity in the XPS spectra of the anode was detected only after 50 cycles in the DETMSA-containing electrolyte. The additive may preferentially deposit on the cathode and, with time, the oxidized products migrate toward the hard-carbon anode and get deposited on the anode surface, which changes the composition and structure of the SEI. The intensity of this peak is increased in the electrode after 100 cycles. The modified SEI provides a stable guard to prolong the life of the batteries.

Impedance spectra of the $NaMO_2$/HC full cell were carried out at different states of charge during the first and the fourth charging processes (**Supplementary Figure S3**) to monitor the resistance during cycling with different electrolytes as presented in **Figure 5A** and **Figure 5A'**. The Nyquist plot is composed of three overlapping semicircles and a straight sloping line at the low-frequency end. The full cell with the DETMSA-contained

electrolyte showed slightly reduced interfacial resistance at any SOC compared to the full cell with the baseline electrolyte. The reduced interfacial resistance enables the cells with the DETMSA-added electrolyte to offer higher capacity and capacity retention, as discussed in **Figure 3A**.

The EIS spectra sets were fitted with the equivalent circuit model as shown in **Figure 5A**. It is composed of R1, in series with 3 parallel R/Q. The values of each component at different SOC of the first and fourth cycles were obtained as presented in **Figure 5B**, b' c, and c' for $NaMO_2$/HC cells with blank and DETMSA-containing electrolytes. Resistance R1 (orange) considered mainly arises from the electrolyte, and the value is below 15 Ω. The first semicircle (corresponding to the R2/Q2 in the equivalent circle) at the highest frequency yields nearly constant and low R2 resistance values (green) over all the first de-sodiation processes with the presence of DETMSA (**Figure 5B'**), lower than those obtained in the additive free cells (**Figure 5B**). This R2 value is almost doubled in the fourth de-sodiation process in the cells with blank electrolytes, while remaining low with the presence of DETMSA as plotted in **Figure 5C** and **Figure 5C**'. The second semicircle at high frequency displays resistance R3 (purple) values that remain lower than 20 Ω during the whole first de-sodiation process, whereas when it reached the fourth de-sodiation step, R3 started with high value in blank and DETMSA electrolytes, ~90 and ~120 Ω, respectively. This number dramatically decreased to below 20 Ω and remained almost constant in the following de-sodiation processes. Considering the differences between the first and fourth de-sodiation processes, the first and second semicircle were likely attributed to the passivation surface layer, R2 and R3 surface resistance between electrolyte, passivation layer, and electrode. The resistance R4 corresponding to the semicircle at high-medium frequency showed a similar trend; it decreased initially with the de-sodiation process and the value later remained almost stable during both the first and fourth cycles. This semicircle likely corresponds to the charge transfer reaction. The presence of DETMSA reduced the total resistance value of the $NaMO_2$/HC full cell.

Compared to the cells assembled with blank electrolyte, the DETMSA-containing electrolyte offered more stable resistance with R1, R2, R3, and R4 values during the first and fourth de-sodiation processes as well as a lower total resistance. It is likely that in the presence of DETMSA, a more robust and less resistive SEI is formed, which is consistent with the XPS discussions. The work highlights the potential benefits for other similar electrolyte additives that contain Si–N bonds such as hexamethyldisilazane (HMDS), heptamethyldisila-zane (HTMDS), N, N-diethylamino trimethylsilane (DEATMS), (trimethylsilyl)isothiocyanate (TMSNCS), and 1-(trimethylsilyl)imidazole (1-TMSI).

CONCLUSION

We provide the initial results of the effect of the addition of DETMSA to the electrolyte in a full-cell sodium-ion battery with a P2-O3 type cathode and a hard-carbon anode; the demonstration is compared with the blank electrolyte (1M $NaPF_6$ in EC: DEC) for the first time. The long-term effect of the electrolyte additives on the SEI components and electrochemical performance are discussed.

The presence of DETMSA is beneficial for the SEI formation by offering more robust and less resistive passivation surface layers, which was validated by XPS and impedance spectra studies. The use of DETMSA as an electrolyte additive maximizes the cycle life to 80% in comparison to the blank electrolyte (40%) by *in situ* scavenging of the harmful H_2O and HF evolved in the battery system during cycling.

DATA AVAILABILITY STATEMENT

The original contributions presented in the study are included in the article/**Supplementary Material**; further inquiries can be directed to the corresponding authors.

AUTHOR CONTRIBUTIONS

LC and BK contributed equally to this work.

FUNDING

The authors thank Innovate UK (IUK PROJECT 104179) and the Horizon 2020 European Union funding for research and innovation (GA No. 963542) for funding.

SUPPLEMENTARY MATERIAL

The Supplementary Material for this article can be found online at: https://www.frontiersin.org/articles/10.3389/fenrg.2022.925430/full#supplementary-material

REFERENCES

Bauer, A., Song, J., Vail, S., Pan, W., Barker, J., and Lu, Y. (2018). The Scale-Up and Commercialization of Nonaqueous Na-Ion Battery Technologies. *Adv. Energy Mat.* 8 (17), 1–13. doi:10.1002/aenm.201702869

Chang, Z., Qiao, Y., Deng, H., Yang, H., He, P., and Zhou, H. (2020). A Stable High-Voltage Lithium-Ion Battery Realized by an In-Built Water Scavenger. *Energy Environ. Sci.* 13, 1197–1204. doi:10.1039/d0ee00060d

Chen, J., Liang, F., Zhang, H., Liu, J., and Li, C. N. (2017). N,N-diethyl-trimethylsilylamine as an Electrolyte Additive for Enhancing Electrochemical Performance of High Voltage Spinel Cathode. *Int. J. Electrochem. Sci.* 12, 7249–7261. doi:10.20964/2017.08.25

Chen, H., Chen, J., Zhang, W., Xie, Q., Che, Y., Wang, H., et al. (2020a). Enhanced Cycling Stability of High-Voltage Lithium Metal Batteries with a Trifunctional Electrolyte Additive. *J. Mat. Chem. A* 8 (42), 22054–22064. doi:10.1039/d0ta07438a

Chen, L., Kishore, B., Walker, M., Dancer, C. E. J., and Kendrick, E. (2020b). Nanozeolite ZSM-5 Electrolyte Additive for Long Life

Sodium-Ion Batteries. *Chem. Commun.* 56, 11609–11612. doi:10.1039/d0cc03976d

Cheng, F., Zhang, X., Qiu, Y., Zhang, J., Liu, Y., Wei, P., et al. (2021). Tailoring Electrolyte to Enable High-Rate and Super-stable Ni-Rich NCM Cathode Materials for Li-Ion Batteries. *Nano Energy* 88 (March), 106301. doi:10.1016/j.nanoen.2021.106301

Eshetu, G. G., Diemant, T., Hekmatfar, M., Grugeon, S., Behm, R. J., Laruelle, S., et al. (2019). Impact of the Electrolyte Salt Anion on the Solid Electrolyte Interphase Formation in Sodium Ion Batteries. *Nano Energy* 55 (September 2018), 327–340. doi:10.1016/j.nanoen.2018.10.040

Fondard, J., Irisarri, E., Courrèges, C., Palacin, M. R., Ponrouch, A., and Dedryvère, R. (2020). SEI Composition on Hard Carbon in Na-Ion Batteries after Long Cycling: Influence of Salts (NaPF6, NaTFSI) and Additives (FEC, DMCF). *J. Electrochem. Soc.* 167 (7), 070526. doi:10.1149/1945-7111/ab75fd

Gorman, S. F., Pathan, T. S., and Kendrick, E. (2019). The 'use-By Date' for Lithium-Ion Battery Components. *Phil. Trans. R. Soc.* A377, 20180299. doi:10.1098/rsta.2018.0299

Han, J.-G., Lee, S. J., Lee, J., Kim, J.-S., Lee, K. T., and Choi, N.-S. (2015). Tunable and Robust Phosphite-Derived Surface Film to Protect Lithium-Rich Cathodes in Lithium-Ion Batteries. *ACS Appl. Mat. Interfaces* 7, 8319–8329. doi:10.1021/acsami.5b01770

Han, J. G., Kim, K., Lee, Y., and Choi, N. S. (2019). Scavenging Materials to Stabilize LiPF6 -Containing Carbonate-Based Electrolytes for Li-Ion Batteries. *Adv. Mat.* 31 (20), e1804822–12. doi:10.1002/adma.201804822

Han, J.-G., Jeong, M.-Y., Kim, K., Park, C., Sung, C. H., Bak, D. W., et al. (2020). An Electrolyte Additive Capable of Scavenging HF and PF5 Enables Fast Charging of Lithium-Ion Batteries in LiPF6-Based Electrolytes. *J. Power Sources* 446 (October 2019), 227366. doi:10.1016/j.jpowsour.2019.227366

Haridas, A. K., Nguyen, Q. A., Terlier, T., Blaser, R., and Biswal, S. L. (2021). Investigating the Compatibility of TTMSP and FEC Electrolyte Additives for LiNi0.5Mn0.3Co0.2O2 (NMC)-Silicon Lithium-Ion Batteries. *ACS Appl. Mat. Interfaces* 13 (2), 2662–2673. doi:10.1021/acsami.0c19347

Herriot, C. (2012). *Entegris, Inc.* Billerica, MA: Note, A. State of the Art. 2–4.

Jiang, X., Liu, X., Zeng, Z., Xiao, L., Ai, X., Yang, H., et al. (2018). A Bifunctional Fluorophosphate Electrolyte for Safer Sodium-Ion Batteries. *iScience* 10, 114–122. doi:10.1016/j.isci.2018.11.020

Kim, D.-H., Kang, B., and Lee, H. (2019). Comparative Study of Fluoroethylene Carbonate and Succinic Anhydride as Electrolyte Additive for Hard Carbon Anodes of Na-Ion Batteries. *J. Power Sources* 423, 137–143. doi:10.1016/j.jpowsour.2019.03.047

Li, Y., Zhang, R., Liu, J., and Yang, C. (2009). Effect of Heptamethyldisilazane as an Additive on the Stability Performance of LiMn2O4 Cathode for Lithium-Ion Battery. *J. Power Sources* 189, 685–688. doi:10.1016/j.jpowsour.2008.08.075

Liao, X.-Q., Zhang, C.-M., Li, F., Yin, Z.-L., Liu, G.-C., and Yu, J.-G. (2021). Dimethyl Trimethylsilyl Phosphite as a Novel Electrolyte Additive for High Voltage Layered Lithium Cobaltate-Based Lithium Ion Batteries. *New J. Chem.* 45 (6), 3160–3168. doi:10.1039/d0nj06010k

Nayak, P. K., Yang, L., Brehm, W., and Adelhelm, P. (2018). Von Lithium- zu Natriumionenbatterien: Vorteile, Herausforderungen und Überraschendes. *Angew. Chem.* 130 (1), 106–126. doi:10.1002/ange.201703772

Peebles, C., Sahore, R., Gilbert, J. A., Garcia, J. C., Tornheim, A., Bareño, J., et al. (2017). Tris(trimethylsilyl) Phosphite (TMSPi) and Triethyl Phosphite (TEPi) as Electrolyte Additives for Lithium Ion Batteries: Mechanistic Insights into Differences during LiNi0.5Mn0.3Co0.2O2-Graphite Full Cell Cycling. *J. Electrochem. Soc.* 164 (7), A1579–A1586. doi:10.1149/2.1101707jes

Sayers, R., Barker, J., and Heap, R. (2018). *United States Patent*. US10550007B2.

Single, F., Horstmann, B., and Latz, A. (2016). Dynamics and Morphology of Solid Electrolyte Interphase (SEI). *Phys. Chem. Chem. Phys.* 18, 17810–17814. doi:10.1039/c6cp02816k

Wotango, A. S., Su, W.-N., Leggesse, E. G., Haregewoin, A. M., Lin, M.-H., Zegeye, T. A., et al. (2017). Improved Interfacial Properties of MCMB Electrode by 1-(Trimethylsilyl)imidazole as New Electrolyte Additive to Suppress LiPF6 Decomposition. *ACS Appl. Mat. Interfaces* 9, 2410–2420. doi:10.1021/acsami.6b13105

Wotango, A. S., Su, W.-N., Haregewoin, A. M., Chen, H.-M., Cheng, J.-H., Lin, M.-H., et al. (2018). Designed Synergetic Effect of Electrolyte Additives to Improve Interfacial Chemistry of MCMB Electrode in Propylene Carbonate-Based Electrolyte for Enhanced Low and Room Temperature Performance. *ACS Appl. Mat. Interfaces* 10 (30), 25252–25262. doi:10.1021/acsami.8b02185

Xu, G., Amine, R., Abouimrane, A., Che, H., Dahbi, M., Ma, Z., et al. (2018). Challenges in Developing Electrodes , Electrolytes , and Diagnostics Tools to Understand and Advance Sodium-Ion Batteries. *Adv. Energy Mater.* 14, 1702403. doi:10.1002/aenm.201702403

Yamane, H., Inoue, T., Fujita, M., and Sano, M. (2001). A Causal Study of the Capacity Fading of Li1.01Mn1.99O4 Cathode at 80°C, and the Suppressing Substances of its Fading. *J. Power Sources* 99, 60–65. doi:10.1016/s0378-7753(01)00479-7

Yan, G., Reeves, K., Foix, D., Li, Z., Cometto, C., Mariyappan, S., et al. (2019). A New Electrolyte Formulation for Securing High Temperature Cycling and Storage Performances of Na-Ion Batteries. *Adv. Energy Mat.* 9, 1901431. doi:10.1002/aenm.201901431

Zhang, L., Min, F., Luo, Y., Dang, G., Gu, H., Dong, Q., et al. (2022). Practical 4.4 V Li||NCM811 Batteries Enabled by a Thermal Stable and HF Free Carbonate-Based Electrolyte. *Nano Energy* 96, 107122. doi:10.1016/j.nanoen.2022.107122

Zhang, S. S. (2006). A Review on Electrolyte Additives for Lithium-Ion Batteries. *J. Power Sources* 162 (July), 1379–1394. doi:10.1016/j.jpowsour.2006.07.074

Zhou, R., Huang, J., Lai, S., Li, J., Wang, F., Chen, Z., et al. (2018). A Bifunctional Electrolyte Additive for H2O/HF Scavenging and Enhanced graphite/LiNi0.5Co0.2Mn0.3O2 Cell Performance at a High Voltage. *Sustain. Energy Fuels* 2 (7), 1481–1490. doi:10.1039/c8se00064f

Conflict of Interest: The authors declare that the research was conducted in the absence of any commercial or financial relationships that could be construed as a potential conflict of interest.

Publisher's Note: All claims expressed in this article are solely those of the authors and do not necessarily represent those of their affiliated organizations, or those of the publisher, the editors, and the reviewers. Any product that may be evaluated in this article, or claim that may be made by its manufacturer, is not guaranteed or endorsed by the publisher.